

Speciation and structure of dipicolinate complexes and Eu(III) ions in solution

Patrick R. Nawrocki*

Received June 2017, Accepted April 2018

Complexation between Eu(III) ions and dipicolinate tridentate ligands (DPA) have been studied to expand on our current understanding of structural and photophysical properties of lanthanides in solution. The dynamic ligand-exchange of labile lanthanide ions, has made it difficult to properly identify the bis ligated Eu(III) complex, as optical spectroscopy only reveals a weighted average of the present species. In this article, evidence for the bis ligated Eu(III) complex will be presented, which is a necessary component in accurately determining the binding constants and to gain further insight in the structure-property relationship of the systems. Additionally, NMR, luminescence spectroscopy and X-ray scattering were used as structural corroboration to further establish the relationship between the solution structure and the intensities of Laporte parity forbidden $f-f$ transitions, characteristic of the lanthanides.

Introduction

f -block elements are essential to our modern society. They have unique optical properties in the form of sharp transitions bands, and their electron configuration makes them exceptional components in magnetic applications.¹ They are also used in the medical field as contrast agents in MRI scans.^{2, 3} Furthermore, understanding the solution chemistry of lanthanides are of great interest in dealing with the nuclear waste problem.⁴ The chemistry of lanthanides, consist almost exclusively of complexation by coordination. This is a result of the 4f orbitals being contracted within the circumference of the 5s orbitals, effectively shielding the valence orbitals from outside interactions.⁵ This phenomenon is the basis for many of the unique properties of lanthanides. Conversely, it also complicates elemental separation, as all lanthanides effectively behave as spheres of varying sizes. The current most effective method of separation is highly polluting, and is currently only done industrially in China.⁶ A greater understanding of lanthanide solution chemistry, will lead to improvements of the separation method, eventually making lanthanides more readily available on a global scale.

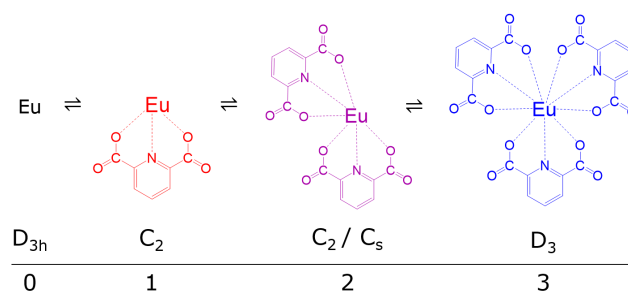


Figure 1 – Scheme of complexation equilibria for EuDPA in the aqueous, mono-, bis- and tris ligated species, with their related symmetries.

For this purpose, constructing and understanding lanthanide model systems as a foundation for lanthanide structure-property relationships in solution, is an essential step in lanthanide solution chemistry studies. For such a model system, Eu(III) is an excellent example because of its non-degenerate 5D_0 emissive state. Lanthanides possess strong spin-orbit coupling⁷ This induces a large separation of absorption and emission bands, preventing spectral overlap in the spectra. Each transition will emit to 7F_J ($J=0-6$) sub-levels of different degeneracies, and can be utilized to deduce structural information of the complex.

Of eligible ligands for this model system, classes such as acetylacetonate,^{8, 9} cyclen-based polydentates^{10, 11} and the tridentate dipicolinates,^{12, 13} are among the most studied. Model systems of cyclen compounds is an active field, but DPA ability to form highly symmetric complexes with 9-coordinate lanthanides, merits its own field of research. Both the fully hydrated and the fully complexed europium ion has so far been reported to have tricapped trigonal prismatic structure in solution,

with D_3 point group symmetry. The mono ligated complex will have a lower C_2 symmetry and the bis ligated is presumed to have C_2 or C_S symmetry, depending on its immediate conformation. A representation of the dynamic equilibria of complexation can be seen in Figure 1.

Here, the foundation for a EuDPA based model system is laid, with the ambition for the model system to be applicable to other LnDPA complexes. So far, three objectives have been accomplished. Initially, a standard for sample preparation is formulated, with the purpose of successfully reproducing previously reported results with spectroscopic techniques. Then an investigation of DPA complex speciation is done. Despite the extensive studies of DPA based lanthanide complexes, the photophysical behaviour of these systems has been described without appropriate identification of the **2** species. Speciation is followed by optical spectroscopy and the trends modelled. Finally, the structure has been determined to confirm the presence of complex species in specific solutions, as predicted by NMR and optical spectroscopy.

Results and Discussion

Several samples were made with varying metal-to-ligand ratios. The 1:0, 1:1, 1:2 and 1:3 samples have been included in all investigations, as reference points to discern the specific properties of the mono, bis and tris DPA complexes. Additional samples have been produced for specific measurements, to probe complex speciation as the solutions shift into a different equilibrium domain. Especially the **2** complex has shown to be difficult to observe.^{12, 13} Preparing the solution samples initially posed a challenge, as complexes of europium hydroxides would form at high pH. Below pH 2, the hydroxide complex was successfully dissolved, and a transparent solution observed, although DPA would start to crash out as dipicolinic acid if left at $\text{pH} < 2$. For 1:0 and 1:3 solution samples, precipitation will not occur. It appeared that the point of solvation for DPA and $\text{Eu}(\text{OH})$, respectively, were overlapping for solutions with lower DPA concentrations than 3 eq. of Eu.

Fortunately, precipitation was not observed until approximately 3 hours after reducing pH below 2 in samples with $20 \mu\text{M}$ $\text{Eu}(\text{III})$, so that measurements could still be made on the samples. Pictures of both precipitate types are shown in SI Figure 1 & 2.

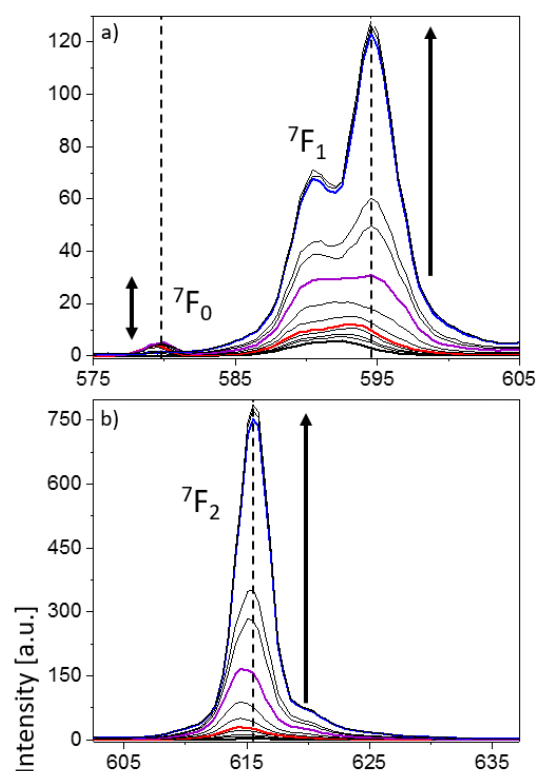
To probe the speciation, a 14 point titration series was made for luminescence and diffraction measurements, with DPA concentrations ranging from 0 to 4 equivalents of metal ion. For the NMR studies, 8 samples were prepared with DPA eq. of 0 to 3. Due to the dynamic equilibria of the complexes and long lifetimes of the lanthanides, the excited states will frequently emit from a different species than the absorbing species. Lifetime data therefore illustrate a weighted average of these species. Therefore, only samples with DPA concentrations with stoichiometric multiples of the metal ions were prepared.

Establishing speciation

The titration series of Eu with DPA has been measured using time-gated emission spectroscopy, and are shown in Figure 2. The emission peaks match the characteristic ${}^5\text{D}_0 \rightarrow {}^7\text{F}_{0-6}$ transitions known for $\text{Eu}(\text{III})$ ions.^{14, 15} The literature describe the

development of the peak intensities as complexation proceeds.^{1,2} Drastic changes in both intensity and crystal-field fine structure arise when the restrictions of the Laporte forbidden $f-f$ transitions are relaxed as DPA coordinates.⁵ The degree to which the Laporte selection rules are relaxed is specific for each distinct transition, and depends on the metal ions local symmetry. Emission spectroscopy can measure the changes in the spectral lines and intensities that are unique to each complex type. The symmetries can then be deduced using Tanner's method of descending symmetry by the crystal-field splitting,⁷ as has been previously established.¹²

By understanding the changes in intensity and crystal-field splitting of the spectral lines, it should be possible to designate specific spectral signatures to each stage of EuDPA complexation. An example of this is the appearance of the ${}^7\text{F}_0$ transition peak in the presence of low symmetry **1** and **2**



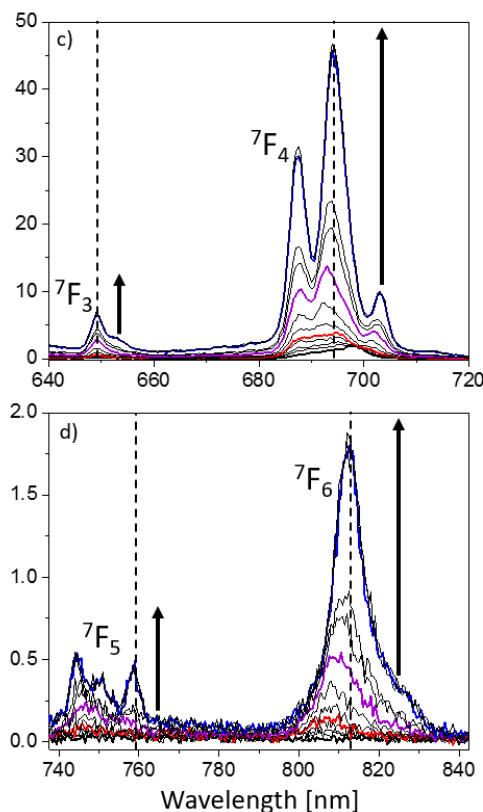


Figure 2 – Time-gated emission spectra of a 14 point titration of 0.02 M Eu(III) ions with increasing DPA concentrations from 0 to 4 equivalents of ligand molecules per metal ion in water. Complexation can be monitored by changes in transition peak intensities and splitting of spectral lines from crystal-field perturbations.

Table 1 – Calculated lifetimes and q for stoichiometric EuDPA solutions.

Eu:DPA	τ H ₂ O [ms]	τ D ₂ O [ms]	q (exp.)	q (lit.) ¹⁶
1:0	0.1	3.9	10.1	-
1:1	0.2	3.2	6.0	-
1:2	0.4	3.0	2.8	2.9
1:3	1.0	3.1	0.5	0.3

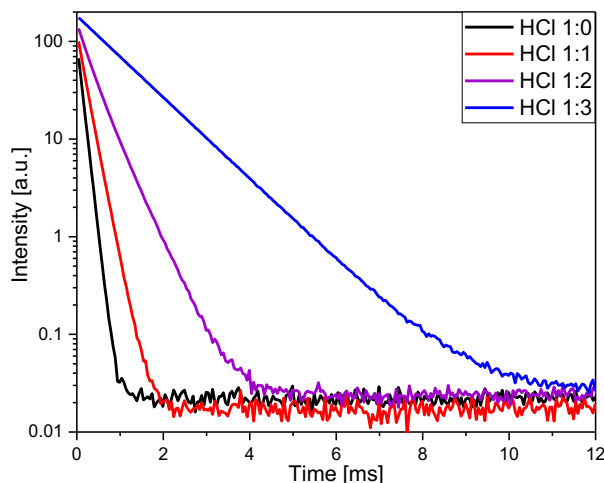


Figure 3 – Lifetimes of EuDPA complexes in H₂O. Inherent uncertainty increases as the lifetime decrease, as is the case of the 1:0 and 1:1 solutions.

complexes, and their consequent disappearance as the complexes shift towards **3**. The luminescence spectra show a definite development for complexation, but emission is unable to probe the distribution of species in solution. This is a consequence of fast ligand exchange rates characteristic of lanthanide metal ions as well as their long lifetimes in the millisecond timescale.

The spectra will therefore show a weighted average of the emissive species present in solution. An insight into the dynamic equilibrium of the solutions has been achieved by measuring the lifetimes of samples with integer multiple concentrations of DPA to europium. By measuring the lifetimes of these samples as well as their deuterated analogues, an approximation of the average number of solvent molecules in the inner coordination sphere can be determined. This can be calculated using the modified Horrocks equation, with the number of inner sphere solvent molecules denoted by q (Eq. 1).¹⁷ The calculation accounts for the greater quenching effect that O-H oscillators have on excited states of europium(III) and terbium(III), as compared to the deuterated analogue of O-D oscillators. The modified Horrocks equation calculates the number of coordinated solvent molecules by considering this difference in quenching efficiency:

$$q = A(k(\text{H}_2\text{O}) - k(\text{D}_2\text{O}) - B) \quad \text{Eq. 1}$$

With $A = 1.2 \text{ ms}^{-1}$ being the proportionality constant, and $B = 0.25 \text{ ms}^{-1}$ a correction for outer sphere effects, both specifically for Eu.¹⁷ The calculated q 's are listed in Table 1 along with previously reported values for the 1:2 and 1:3 solutions. In the absence of DPA, the hydration number of the 9-coordinate Eu(III) ion should be 9. For each added ligand, q should decrease by 3, with $q = 0$ when no water is present in the inner sphere, when the tris complex is achieved. Calculated q for the 1:3 solution is 0.5 and shows that the equilibrium is shifted towards **3** to a high degree, yet the solution does not consist entirely of this specie alone. This is in agreement with europium(III) ions forming labile complexes rapid ligand exchange. During ligand exchange, it is possible for water molecules to coordinate briefly, increasing the average value of q . It should be noted that while q is efficient at approximating the hydration number, the method has some inherent uncertainty when measuring solutions with short lifetimes. As is the case for fully hydrated Eu in H₂O as seen in Figure 3, and from the calculated q of 10.1 from Table 1.

The complexation can be monitored via q and by the intensities and splitting of J-sublevels of transition bands. Tanner's diagram of descending symmetry correlates the J-sublevel splitting with the symmetry of each complex species⁷. The same development was observed by NMR spectroscopy. Samples of varying Eu:DPA ratios were measured with ¹H-NMR spectroscopy as shown in Figure 4.

An advantage of NMR measurements of most lanthanide based complexes, are the large chemical shifts arising from paramagnetic Eu(III). The ¹H-NMR spectra of the titration series help to further facilitate the presence of each complex species. In the spectra of the EuDPA complexes, two peaks appear to be from the complex: one shifting from about 2.5 to 3.7 ppm, and another from 4.4 to 4.8 ppm. The large peak coming from water at 4.7 ppm overlap with the most shifted DPA peak, and should be suppressed in further studies. The peak of DPA is presumed to

reflect the hydrogen atoms of the para- and meta-positions compared to the nitrogen atom of pyridine. Another possibility could be that both hydrogen atoms are represented simultaneously within the peaks, and that the peaks instead represent the averages of coordinated versus uncoordinated DPA. This could be established by using a DPA derivative with a substituent group with no hydrogens, in the para position of the nitrogen atoms.

NMR spectroscopy operate on the microsecond timescale. As ligand exchange rates of the complexes occur closer to the nanosecond timescale, the NMR spectra will portray a weighted average of the present species. On this basis, shifting of the peak

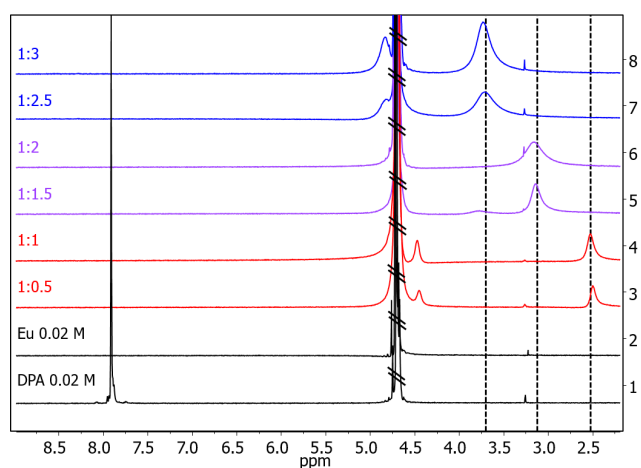


Figure 4 – Paramagnetic ^1H -NMR spectroscopy of EuDPA titration of 0.02 M Eu with equivalent DPA concentrations as shown on the figure. Both complex peaks show periodic shifts instead of a gradual migration, indicative of a single equilibrium being dominant in a given solution. The sharp water peak at 4.7 overlaps with the most shifted complex peak, why the peak shift between the 1:1.5 to 1:2.5 solutions is difficult to observe.

would be expected to be gradual if every equilibrium between the 0, 1, 2 and 3 complexes were expressed simultaneously. Instead, the peak shift are observed to be systematic, as spectra of the 0.5, 1.5 and 2.5 eq. Eu:DPA solutions are near identical to those of the 1, 2 and 3 eq. solutions, respectively. It can be assumed that each of these intermediate stoichiometric solutions, will assume the same dominant equilibrium, as the subsequent stoichiometric solution operates within. This agrees with the prediction, that the equilibrium of the 0.5 eq. solution as well as the 1 eq., is dominated by $\text{Eu}^{3+} + \text{DPA}^{2-} \rightleftharpoons \text{Eu}(\text{DPA})^+$. When the ligand concentration surpasses that of the metal ion, the $\text{Eu}(\text{DPA})^+ + \text{DPA}^{2-} \rightleftharpoons \text{Eu}(\text{DPA})_2^-$ start to become the prevalent equilibrium, of which the trends continues for $\text{Eu}(\text{DPA})_2^- + \text{DPA}^{2-} \rightleftharpoons \text{Eu}(\text{DPA})_3^{3-}$. A few points of interest could be explored further, such as probing the threshold at which a new dominant equilibrium is established, by expanding the titration series. Additionally, interchanging the paramagnetic europium complex core with a diamagnetic yttrium ion will help us understand the paramagnetic influence.

Electronic transitions in Eu(III)

Before proceeding to the discussion of europium(III)-based complexation, a short outline of the electronic properties of the metal ion is required, to justify the connection made between

spectral results and the structure in solution.

Within the field of lanthanide photophysics, transition intensities of optical spectroscopy are commonly described by Judd-Ofelt theory.^{18, 19} The theory attempts to express intensities in terms of dipole strengths and are calculated based on experimentally determined parameters. While the theory is capable of approximating the transition intensities, calculated intensities often differ from the experimental values by up to 15 %.¹³

This intrinsic uncertainty of the theory has prompted the use of the more fundamental Laporte selection rules as a framework. Rather than determining the exact intensities, the selection rules are used for predicting certain trends in transition bands.

For Eu(III), the $^5\text{D}_0 \rightarrow ^7\text{F}_{0,6}$ transitions are induced electric dipoles, save for the magnetic dipole transition of $^5\text{D}_0 \rightarrow ^7\text{F}_1$. They are induced transitions compared to standard electric dipole transitions, with much weaker intensities, as dictated by the parity rule. When a crystal-field perturbation is introduced, parity mixing is possible and the number of available Stark sublevels increase.

A correlation between the symmetry system and the quantum number J to determine the number of available Stark levels has been reported.²⁰ Selection rules for f - f transitions are listed according to symmetry by Tanner. The correlations between different transitions of $^5\text{D}_0 \rightarrow ^7\text{F}_{0,6}$ and the solution symmetry can be extrapolated, and has been constructed by mathematical treatment of these phenomena.

The selection rules predict stronger intensities for induced electric dipole transition $^5\text{D}_0 \rightarrow ^7\text{F}_J$ of $J = 2, 4$ and 6 , and weak intensities for $J = 0, 3$ and 5 . Noticeably, the $^5\text{D}_0 \rightarrow ^7\text{F}_2$ induced electric dipole transition follows the selection rule of an electric quadrupole transition. These so-called pseudo-quadrupole transitions are known for their hypersensitivity to the local environment, by which immense intensity increases in the transition band can be observed. By use of crystal-field splitting, changes in intensities and the aforementioned diagram of descending symmetry by Tanner, the

Table 2 – Selection rules generated on the basis of Laporte's parity rule

Operator	Parity	ΔS	ΔL	ΔJ
ED	Opposite	0	≤ 6	≤ 6 (2,4,6 if J or J'=0)
MD	Same	0	0	$0, \pm 1$
EQ	Same	0	$0, \pm 1, \pm 2$	$0, \pm 1, \pm 2$

correlations between different transitions of $^5\text{D}_0 \rightarrow ^7\text{F}_{0,6}$ and the solution symmetry can be extrapolated. The transitions for Eu(III) has been described by Binnemans.¹⁵ Some of the clearer trends include the high-symmetry dependant $\Delta J = 0$, and the $\Delta J = 1$ magnetic dipole transitions that is assumed to be insensitive to the environment¹⁵. Conversely, the $\Delta J = 2$ hypersensitive transition is very susceptible to its local environment. It has been shown experimentally that the intensity of $\Delta J = 2$ is related to the degree of covalency between metal and ligand, according to Judd-Ofelt theory.²¹

The $^5\text{D}_0 \rightarrow ^7\text{F}_{3,6}$ transitions show less clear trends and will not be attempted to be generalised in the same manner at this point.

Speciation modelling

The empirical data presented from the emission spectra, hydration numbers and NMR spectra, show evidence for

signatures specific to each complex type, including the bis complex. The trends observed from the emission spectra can be used as a foundation for speciation modelling. Luminescence spectroscopy can probe a system on a time-scale reflecting the lifetimes of the complexes that are measured. For these complexes, the timescale is in the microsecond timescale, similar to NMR. The emission data is therefore also a result of a weighted average of present species. In particular, **2** becomes difficult to distinguish from the emission spectra. If the complex signatures are expressed in terms of transition band intensities, the trends become more pronounced. The intensities have been plotted as isotherms in Figure 5a. The isotherms of the intensities show a significant increase upon complexation. This is primarily an effect of relaxed selection rules. To a lesser degree it is due to fewer interacting O-H oscillators available to quench the europium excited states. Noticeably for the 7F_0 isotherms, the magnitude of the intensities decreases as the DPA concentration surpass 2 equivalents of the metal ion, as symmetry starts to reform.

Figure 5b show the relative intensities of the transitions opposed to the environmentally stable magnetic dipole transitions. The changes in the 7F_1 transition are small, and can be neglected for the current purpose. Division by the stable 7F_1 intensity eliminates the variance created by the increase in the total intensity. The plots showing the intensity ratios describe the symmetry-dependant behaviour of the transitions in a clear way. The model describes the data well, but the fit can be improved by increasing the number of titration points in the series. With the currently presented data, the finer details are lost.

The intensive isotherms describing the mono complex are the $\Delta J = 0$ and 4 transitions. The bis complex is indicated by the $\Delta J = 3$ and 6 transitions, and the tris complex by the $\Delta J = 2, 3, 4$ and 5 transitions. Using the DynaFit software to fit these trends, the association constants for each complex has been modelled and tabulated in Table 3, with association constants from literature for reference.^{22, 23} The ${}^7F_2 / {}^7F_1$ intensive isotherm has been excluded to improve the current model fit.

Table 3 – Binding constants obtained by model fitting of isotherms using DynaFit software.

Binding constants	Experimental	Literature ²²
$\beta_1 = [1]/[0][DPA]$	4.4e8	5.01e8
$\beta_2 = [2]/[1][DPA]$	2e8	1.26e8
$\beta_3 = [3]/[2][DPA]$	1.3e8	3.99e5

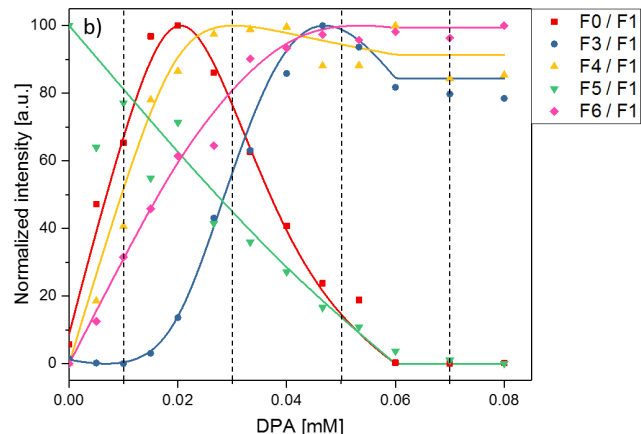
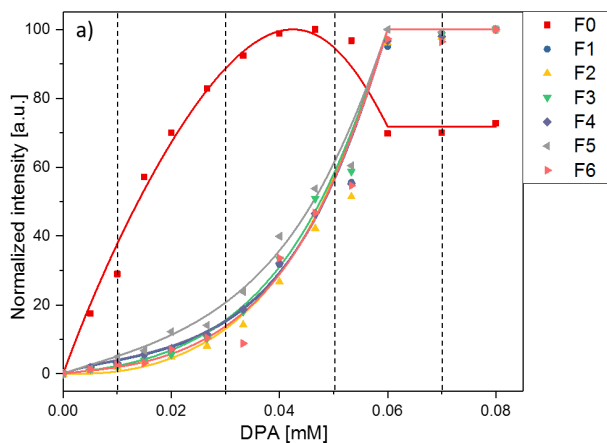


Figure 5 – Normalized intensity isotherm plots as a function of added DPA ligand. Isotherms of a) show the development of the intensities themselves, of which only the ${}^5D_0 \rightarrow {}^7F_0$ transition changes irregularly. The intensive isotherms of b) show much more pronounced changes upon complexation. The ${}^5D_0 \rightarrow {}^7F_2$ transition of the intensive isotherms is left out, as the inclusion in the data fit result in a poor model.

The isotherm should be included when a titration series with many additional EuDPA ratio increments has been made.

Structure determination

With the techniques presented, speciation of EuDPA complexes has been provided, and binding constants for each equilibrium determined.

As has been discussed, results from 1H -NMR and optical spectroscopy mainly reveal the speciation of complexation, due to weighted average data from millisecond timescales. Structural information available from the emission data could potentially be elaborated upon more carefully by use of the symmetry-based trends presented for Eu's electronic transitions. Analysing the spectral intensities and crystal-field splitting could reveal much about the local symmetry of the complex, especially if done in conjunction with absorption spectra. In contrast to the millisecond timescale emission and NMR spectroscopy methods, absorption spectroscopy measures data on the femtosecond timescale,²⁴ probing the instantaneous environment.

In this project, probing of the instantaneous environments has been attempted using X-ray diffraction data, a method also operating on the femtosecond time-scale.²⁵ Additionally, X-ray scattering can directly reveal the complex structure from treated diffraction data, even for solution structure.

X-ray scattering

Discerning structural information using X-ray scattering has the advantage of probing the instantaneous environment of the sample,²⁶ instead of giving a weighted average representation. Diffraction patterns arise when X-rays interact with electrons of a sample, effectively scattering the photons. Scattered photons interact with each other as they propagate through space. The interference pattern (scattering intensity as function of scattering angle) thus contain information about the position of atoms in a sample. The diffractions patterns will emerge when the

interference of waves satisfy Bragg's Law, and show up as intensities on the detector.

$$n\lambda = 2d \sin(\theta) \quad \text{Eq. 2}$$

These intensities are proportional to the distribution of electron density of atoms within the unit cell of a structure, called the structure factor.

$$I \propto |F|^2 \quad \text{Eq. 3}$$

The structure factor sums over the electron densities of each atom in the unit cell, described by the form factor, f , which itself is proportional to the number of electrons in an atom. Another significant part of the structure factor is the Debye-Waller factor that accounts for thermal motion of atoms.

The Pair Distribution Function (PDF) is achieved when total scattering data collected in Q-space is corrected and converted to a real space function²⁷. The PDF has the advantage of illustrating the data as a function of r , essentially creating a histogram of interatomic distances that are intuitively easier to interpret.

Total scattering includes both standard Bragg scattering as well as Thomson scattering. After subtracting background scattering and correcting for incoherent scattering from the raw data, the coherent scattering function $I(Q)$ is formed. This function is normalized according to the mean squared form factor, creating the total scattering structure function.

$$S(Q) = \frac{I(Q) - \langle f(Q)^2 \rangle + \langle f(Q) \rangle^2}{\langle f(Q) \rangle^2} \quad \text{Eq. 4}$$

The structure function is the normalized scattering function that oscillates around 1. By subtracting $S(Q)$ by 1 and multiplying the term with Q , the weight of intensities at high Q -values will be amplified, and the function will oscillate around 0. Finally, a Fourier transformation will convert the Q -space function into real space in the shape of the PDF, $G(r)$.

$$G(r) = \frac{2}{\pi} \int_0^\infty F(Q) \sin(Qr) dQ \quad \text{Eq. 5}$$

Table 4 – Characteristic interatomic distances assigned the PDF peaks in Figure 6.

r [Å]	Atomic pairs
1.25	C – O (Carboxylic)
1.3	C = C (Pyridine neighbours)
2.4	Eu – O
2.5	C – C (Pyridine meta)
2.7	Eu – N
2.7	C – C (Pyridine Para)
2.7	C – N (Pyridine Para)
3.4	Eu – C (Carboxylic)
4.6	Eu – O (Oxo)
5.2	Eu – C (Para to nitrogen)

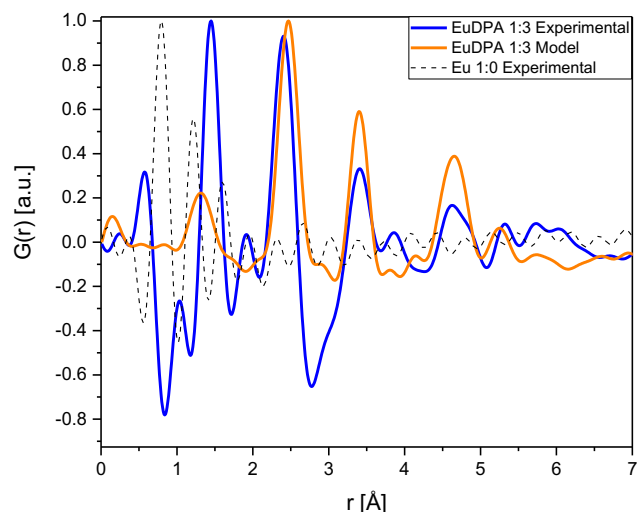


Figure 6 – Normalized PDF of experimental data versus calculated interatomic distances. Model and experimental data of the 1:3 complex is in moderate agreement and confirm the presence of the complex.

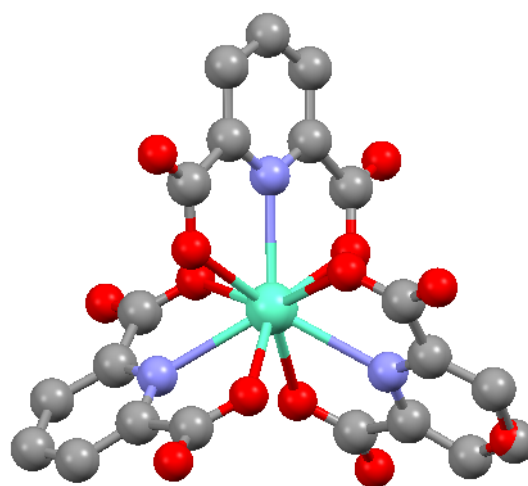


Figure 7 – Crystal structure of $\text{Eu}(\text{DPA})_3 \cdot 3$.

The function essentially serves as a histogram of interatomic distances in the sample. Studying interatomic distances using PDF has gained much traction over the last couple of decades.^{28, 29} Standard crystallographic methods have been limited to study only materials with long range structure, but high flux synchrotrons with large X-ray energies can achieve high Q -space data. This allows local atomic structure to be studied. Here, we use total scattering and PDF to study structure in solution. The PDF illustrated in Figure 6 show the structural information of a 1:3 ratio solution, along a model of the expected PDF, as well as a 0.2 M Eu sample with poor data as reference. A structural illustration of the tris complex can be seen on Figure 7. To stay in accordance with reported literature, the samples were initially prepared with 20 mM Eu(III), to minimize changed parameters. Based on the diffraction data, the sample concentrations were too low to distinguish complex related distances from solvent background in the X-ray scattering data. A selection of samples were remade at the synchrotron with higher concentrations. Clear features are observed for the 100 mM 1:3 sample. A cursory inspection of Table 4 shows the assignments for specific

atomic pair distances in the complex. Many of the distances found, are in agreement with crystallographic data reported of a $\text{Eu}(\text{DPA})_3^{-3}$ crystal structure of the complex.³⁰ The experimental data of **3** have similar pronounced features as the calculated PDF, yet a general discrepancy between model and experimental data can be observed throughout the PDF's. Most noticeable is the peak at about 1.4 Å that is shifted slightly to longer distances in the experimental PDF.

The PDF study suggests the presence of **3**, but is currently inconclusive in several aspects of the study. Nevertheless, a greater understanding of the complex' chemistry has been achieved, and of the concentration limitations that must be dealt with when using X-ray scattering.

Conclusion

The aim of this project was to reproduce data previously presented in the literature, and subsequently identify the **2** complex species in solution and thereby incorporate in speciation modelling.

The EuDPA complexes has successfully been made, along with a method useable for reproducing every point in a titration series with no precipitation observed 3 hours after mixing.

Luminescence and NMR spectroscopy has enabled us to observe and monitor the complexation of europium with dipicolinate as $\text{Eu}(\text{DPA})_3^{-3}$. This serves to establish a foundation for researching lanthanide complexes using dipicolinate ligands within our research team. With optical spectroscopy, the development of the crystal-field perturbations could be followed. By fitting the isotherms, the spectral changes could be modelled and the binding constants of the three equilibria determined. β_1 and β_2 in particular are comparable to those reported in the literature, while β_3 were about 3 orders of magnitude larger. The intensive isotherms clearly show that **2** is influencing the spectral intensities, effectively confirming its participation in the complex' equilibria.

The presence of **2** is corroborated by the ^1H -NMR titration series, from which each equilibrium domain was clearly probed, while the hydration numbers calculated from complex excited state lifetimes, further indicate the shifted equilibrium of the complex species.

Finally, the presented PDF is indicative of the solution structure expected of **3**, but the total scattering experiments are currently inconclusive, and will continue in further studies.

In summary, the project has been successful in pinpointing the bis complex species and determining the binding constants of the equilibria. Additionally, proof-of-concept of the lanthanide complex structure-property relationship has been outlined. The identification of the **2** species should emphasize, that revisiting the already established photophysical behaviour of lanthanides in this model complex systems, will add valuable knowledge to our understanding of lanthanide properties.

Experimental

The synthesis of all complex solutions with varying metal to ligand ratios, follow the procedure described in the original work

of Binnemans and Görler-Walrand.¹² However, samples with Eu:DPA ratios around 1:2 tend to precipitate. This prompted the devising of a more synthesis route that could be dependably reproduced. This is especially necessary for samples with DPA contents close to 2 equivalents per Eu ion, as precipitation readily took place.

The complications experienced when making the samples, included dipicolinic acid precipitating approximately 3 hours after mixing, creating a flaky precipitate. At higher pH, europium hydroxides form, which appears as a foggy white precipitate. To reproduce results made in the original literature, the metal ion concentrations were standardized at 0.02 M Eu, and DPA contents ranging from 0 to 4 equivalents. For each sample, a 0.1 M Eu stock solution was made by dissolving Eu_2O_3 in 10 % HClO_4 or 2.38 M HCl/DCl . For each sample, appropriate amounts of DPA were weighed and dissolved in 2.38 M NaOH equal to one fifth of the final volume. When both solutions had properly dissolved, the Eu solution was added to the DPA solution in a 1:1 ratio, after which precipitate of the hydroxide complex should form. This leaves 3/5 of the intended final volume, to dissolve precipitate by pH adjustments. If any flaky DPA precipitate hasn't dissolved after mixing, pH is increased. This is done using 4 M NaOH in 20 μl addition. When only the foggy precipitate of the hydroxide complex is present, pH can be cycled back down below pH 2. A clear solution should be observed. The specific limits of solubility were not determined, but the dipicolinic acid was dissolved at pH = 8, while the europium hydroxides were dissolved at pH = 2. A dilution series of the DPA solution would make the procedure much more efficient, but precipitate was difficult to control, after which this method was terminated.

The samples could be made in the exact same manner using HCl or DCl in place of HClO_4 .

Acknowledgement

I would like to thank the entire TJS lanthanide research team of the Nano Chemistry group, whose experience has helped me immensely to understand the field for this thesis. Dr. Riikka Arppe in particular has invested a lot of time in helping me understand the spectroscopic methods I have used. My supervisor Associate Professor Thomas Just Sørensen's enthusiastic encouraging and unwavering faith in me, has made it easy to stay motivated during the project. Lea and Nicolaj, my fellow undergraduate students, has provided endless moral support during late nights at the office.

Special thanks to Assistant Professor Kirsten M. Ø. Jensen and her structure determination group for assisting me in all respects in the field of scattering. Her undergraduate student Emil Kjær's understanding of scattering phenomena has succeeded when my own fell short. I would also like to thank MSc Nina Salinas from the BWL group for repeatedly noticing the times I was lost in the lab.

Finally, special thanks go to my Nanoscience study group. They have helped me stay focused during the project, and have when necessary, offered constructive criticism among other types of criticism.

Notes and references

Address: Nano-Science Center & Department of Chemistry, University of Copenhagen, Universitetsparken 5, 2100 København Ø, Denmark.; E-mail: skf209@alumni.ku.dk

† Electronic Supplementary Information (ESI) available: [details of any supplementary information available should be included here]. See DOI: 10.1039/b000000x/

1. S. Liu, D. Lee, M.-q. Huang, A. Higgins, Y.-h. Shen, Y. He and C. Chen, *Journal of Iron and Steel Research, International*, 2006, **13**, 123-135.
2. S. Faulkner and O. A. Blackburn, *The Chemistry of Molecular Imaging*, 2014, **179-197**.
3. P. Caravan, *Chemical Reviews*, 1999, **99**, 2293-2352.
4. B. J. Mincher, G. Modolo and S. P. Mezyk, *Solvent Extraction and Ion Exchange*, 2009, **27**, 579-606.
5. M. Weller, T. Overton, J. Rourke and F. Armstrong, *Inorganic Chemistry*, OUP Oxford, 2014.
6. Y. Guoan, H. Hui, L. Rushan and Z. Wenbin, *Procedia Chemistry*, 2012, **7**, 215-221.
7. P. A. Tanner, *Springer Ser. Fluoresc.*, 2011, **7**, 183-234.
8. N. P. Kuzmina, L. I. Martynenko, N. V. Chugarov, I. G. Zaitseva, A. N. Grigoriev and A. N. Yakushevich, *Journal of Alloys and Compounds*, 2000, **308**, 158-162.
9. J. Rydberg and Y. Albinsson, *Solvent Extraction and Ion Exchange*, 1989, **7**, 577-612.
10. M. Tropiano, O. A. Blackburn, J. A. Tilney, L. R. Hill, M. P. Placidi, R. J. Aarons, D. Sykes, M. W. Jones, A. M. Kenwright, J. S. Snaith, T. J. Sørensen and S. Faulkner, *Chemistry – A European Journal*, 2013, **19**, 16566-16571.
11. M. Tropiano, O. A. Blackburn, J. A. Tilney, L. R. Hill, T. J. Sørensen and S. Faulkner, *J. Lumines.*, 2015, **167**, 296-304.
12. K. Binnemans, K. VanHerck and C. GorllerWalrand, *Chem. Phys. Lett.*, 1997, **266**, 297-302.
13. M. H. V. Werts, R. T. F. Jukes and J. W. Verhoeven, *Phys. Chem. Chem. Phys.*, 2002, **4**, 1542-1548.
14. W. T. Carnall, G. L. Goodman, K. Rajnak and R. S. Rana, *The Journal of Chemical Physics*, 1989, **90**, 3443-3457.
15. K. Binnemans, *Coord. Chem. Rev.*, 2015, **295**, 1-45.
16. E. G. Moore, *Dalton Trans.*, 2012, **41**, 5272-5279.
17. A. Beeby, I. M. Clarkson, R. S. Dickins, S. Faulkner, D. Parker, L. Royle, A. S. de Sousa, J. A. Gareth Williams and M. Woods, *Journal of the Chemical Society, Perkin Transactions 2*, 1999, DOI: 10.1039/A808692C, 493-504.
18. B. R. Judd, *Physical Review*, 1962, **127**, 750-&.
19. G. S. Ofelt, *J. Chem. Phys.*, 1962, **37**, 511-&.
20. G. K. J. B. Liu, *Tsinghua University Press & Springer*, 2005.
21. C. K. Jørgensen and R. Reisfeld, *Journal of the Less Common Metals*, 1983, **93**, 107-112.
22. J. C. G. Bünzli and A. S. Chauvin, *Spectroscopy Letters*, 2004, **37**, 517-532.
23. I. Grenthe, *J. Am. Chem. Soc.*, 1961, **83**, 360.
24. T. Kowall, F. Foglia, L. Helm and A. E. Merbach, *Journal of the American Chemical Society*, 1995, **117**, 3790-3799.
25. A. Barty, C. Caleman, A. Aquila, N. Timneanu, L. Lomb, T. A. White, J. Andreasson, D. Arnlund, S. Bajt, T. R. M. Barends, M. Barthelmess, M. J. Bogan, C. Bostedt, J. D. Bozek, R. Coffee, N. Coppola, J. Davidsson, D. P. DePonte, R. B. Doak, T. Ekeberg, V. Elser, S. W. Epp, B. Erk, H. Fleckenstein, L. Foucar, P. Fromme, H. Graafsma, L. Gumprecht, J. Hajdu, C. Y. Hampton, R. Hartmann, A. Hartmann, G. Hauser, H. Hirsemann, P. Holl, M. S. Hunter, L. Johansson, S. Kassemeyer, N. Kimmel, R. A. Kirian, M. Liang, F. R. N. C. Maia, E. Malmerberg, S. Marchesini, A. V. Martin, K. Nass, R. Neutze, C. Reich, D. Rolles, B. Rudek, A. Rudenko, H. Scott, I. Schlichting, J. Schulz, M. M. Seibert, R. L. Shoeman, R. G. Sierra, H. Soltau, J. C. H. Spence, F. Stellato, S. Stern, L. Struder, J. Ullrich, WangX, G. Weidenspointner, U. Weierstall, C. B. Wunderer and H. N. Chapman, *Nat Photon*, 2012, **6**, 35-40.
26. T. Egami and S. J. L. Billinge, *Elsevier*, 2012, **Pergamon Materials Series**.
27. S. J. L. Billinge, *Department of Applied Physics and Applied Mathematics, Columbia*.
28. K. M. Ø. Jensen, M. Christensen, P. Juhas, C. Tyrsted, E. D. Bojesen, N. Lock, S. J. L. Billinge and B. B. Iversen, *Journal of the American Chemical Society*, 2012, **134**, 6785-6792.
29. N. Lock, M. Christensen, K. M. Ø. Jensen and B. B. Iversen, *Angew. Chem., Int. Ed.*, 2011, **50**, 7045.
30. P. A. Brayshaw, J. C. G. Bünzli, P. Froidevaux, J. M. Harrowfield, Y. Kim and A. N. Sobolev, *Inorg. Chem.*, 1995, **34**, 2068.